Prangé, *Icarus* **97**, 26 (1992).
5. R. Prangé *et al.*, *J. Geophys. Res.* **98**, 18779 (1993).
6. J. C. Gérard, V. Dols, F. Paresce, R. Prangé, *ibid.*, p. 18793.
7. The overall sensitivity of the optical system is 4.1 × 10^{-6} counts per pixel per second for every kilorayleigh of H_2 Lyman emission. These observations were made before the addition of the Corrective Optics Space Telescope Axial Replacement (COSTAR), so the aberration of the HST primary mirror spread the light of a point source over a circular halo 2 arc sec in radius. All exposures (896 s each) described here were made with the use of the same guide star for telescope pointing and tracking. The center of the camera field of view was located along the planet's central meridian at 60°N during each image.
8. F. W. Harris, personal communication.
9. The precise location of the planetary limb in the FOC field of view was determined from both the near-UV exposure (Table 1), which shows no auroral emission, and from the well-defined limb on each 153-nm auroral image.
10. V. Dols, J. C. Gérard, F. Paresce, R. Prangé, A. Vidal-Madjar, *Geophys. Res. Lett.* **19**, 1803 (1992).
11. The bulk of the H_2 Lyman emissions are emitted in bands near 160 and 161 nm and are optically thin in H_2. Because the northern auroral oval is offset from the rotational pole, the effect of the slant path brightening is reduced somewhat by smearing during the exposure. During a typical exposure of 15 min, the planet rotates by about 9° of longitude. The slant path enhancement is also reduced if the actual auroral structure is unresolved by the FOC. A resolution of about 0.1 arc sec implies that structures smaller than about 400 km are diluted. For comparison, the scale height near the homopause on Jupiter is likely to be about 100 km or so, and a degree of latitude at 60°N subtends about 600 km. We assumed that the aurora's vertical emission rate can be represented by a Chapman profile, used the nominal value of 100 km for the atmospheric scale height and an auroral height of 500 km above the cloud tops, and accounted for the dilution caused by the spatial resolution of the FOC (but not for smearing from the rotation of Jupiter).
12. J. C. Gérard, V. Dols, R. Prangé, F. Paresce, *Planet. Space Sci.*, in press.
13. J. Caldwell, B. Turgeon, X.-M. Hua, *Science* **257**, 1512 (1992).
14. This value can be considered as a lower limit because the aberrated point spread function of the telescope and the blurring effect of the planetary rotation spreads the light of a point source over many pixels and decreases the apparent emission rate of localized emission. A rough estimate of this effect may be obtained from the deconvolved (Wiener) version of Fig. 2A, although this method does not necessarily provide correct photometric values. The brightest region in this case reaches ~10 MR of H_2 Lyman emission.
15. J. C. Gérard and V. Singh, *J. Geophys. Res.* **87**, 4525 (1982).
16. H. J. Waite *et al.*, *ibid.* **88**, 6143 (1983).
17. D. Rego, R. Prangé, J. C. Gérard, *ibid.* **99**, 17075 (1994).
18. The results of the 1 W m^{-2} aurora excited by electrons with the Ulysses energy spectrum imply an H_2^+ production rate exceeding 2 × 10^6 cm^{-3} with a peak production expected near the 1-μbar pressure level and a peak H_3^+ density on the order of 10^8 cm^{-3}. The corresponding heating rate also peaks at this pressure with a vertically integrated heat flux of over 450 ergs cm^{-2} s^{-1}. The heating rate profile calculated from the model can be combined with recent cooling rate calculations (scaled so that the vertically integrated cooling rate equals the vertically integrated heating rate and peaks at a pressure level of 1 μbar, just above the methane homopause, that is, cool-to-space approximation). These values were used as inputs in a 1D thermal conduction equation (*26*) to estimate the auroral thermal profile.
19. L. M. Trafton, J. C. Gérard, G. Munhoven, J. H. Waite, *Astrophys. J.* **421**, 816 (1994).
20. P. Drossart *et al.*, *J. Geophys. Res.* **98**, 18803 (1993).
21. J. T. Clarke *et al.*, *Astrophys. J. Lett.* **430**, 73 (1994).
22. G. R. Gladstone and T. Skinner, *NASA SP-494* (1989), pp. 221–228.
23. M. Hammond and J. Gosling, personal communication.
24. M. K. Dougherty, D. J. Southwood, A. Balogh, E. J. Smith, *Planet. Space Sci.* **41**, 291 (1993); R. Prangé, M. Dougherty, M. Dunlop, A. Balogh, V. Dols, *Eos* **74**, 43 (1993).
25. V. Vasyliunas, *Geophys. Res. Lett.* **21**, 401 (1994).
26. H. J. Waite, M. L. Chandler, R. V. Yelle, B. R. Sandel, T. E. Cravens, *J. Geophys. Res.* **93**, 14295 (1988).
27. J. E. P. Connerney, in *Planetary Radio Emission III*, H. Rucker, M. L. Kaiser, S. J. Bauer, Eds. (Austrian Academy of Sciences Press, Vienna, 1992), pp. 13–33.
28. J.C.G. acknowledges support from the Belgian National Fund for Scientific Research (FNRS) and from the Belgian Federal Science Policy Office, Prime Minister's Services. R.P. is grateful to J. Gosling, M. Hammond, K. Maeda, H. Oya, and P. Zarka for fruitful discussions and for having kindly provided unpublished data on the Jovian radio emission and on the solar wind. She acknowledges partial support of this study by grant INSU-PNP/80374200. J.H.W. acknowledges support from Space Telescope Science Institute grant GO-4608.02-92A and National Aeronautics and Space Administration (NASA) Planetary Atmosphere grant NAGW-3624. This study is based on observations with the NASA-ESA HST that were obtained at the Space Telescope Science Institute, which is operated by AURA for NASA under contract NAS5-26555.

11 July 1994; accepted 27 September 1994

In Situ Determination of the NiAs Phase of FeO at High Pressure and Temperature

Yingwei Fei and Ho-kwang Mao

In situ synchrotron x-ray diffraction measurements of FeO at high pressures and high temperatures revealed that the high-pressure phase of FeO has the NiAs structure (B8). The lattice parameters of this NiAs phase at 96 gigapascals and 800 kelvin are a = 2.574(2) angstroms and c = 5.172(4) angstroms (the number in parentheses is the error in the last digit). Metallic behavior of the high-pressure phase is consistent with a covalently and metallically bonded NiAs structure of FeO. Transition to the NiAs structure of FeO would enhance oxygen solubility in molten iron. This transition thus provides a physiochemical basis for the incorporation of oxygen into the Earth's core.

Ferrous oxide is a basic oxide component in the interior of the Earth. Its high-pressure and high-temperature behavior plays an important role in mantle composition and core formation models. Since shock wave studies (*1*) revealed the existence of a high-pressure phase of FeO at pressures above 70 GPa over a decade ago, the structure of this phase has been the subject of speculation (*1–4*). Transition to this phase has not been observed in static compression experiments in the diamond-anvil cell up to 120 GPa at room temperature (*5*). Additional shock compression experiments (*6*) have confirmed that the density of FeO changes at 70 GPa. The discrepancy between the static and shock compression experiments may be related to the experimental temperature difference in the two techniques. In this study, we report static high-pressure and high-temperature experiments on FeO that resolve this discrepancy. In addition, in situ synchrotron x-ray measurements reveal the structure of the high-pressure, high-temperature phase of FeO. We discuss implications of the high-pressure structure of FeO for the incorporation of oxygen (in the form of FeO) into the Earth's core and for the mineralogy of the lower mantle.

We have developed an externally heated high-temperature diamond-anvil cell (*7, 8*) that is capable of achieving pressures greater than 125 GPa at temperatures up to 1100 K in a mildly reducing atmosphere (Ar with 1% H_2). We conducted experiments on FeO by using this high-temperature cell combined with in situ synchrotron x-ray diffraction measurements. At room temperature, we confirmed the transition from the cubic (B1) to a rhombohedral phase at 16 GPa under hydrostatic conditions (*5*) (Fig. 1). The transition occurs at much lower pressure (~8 GPa) when no pressure medium is used in the experiments. High-temperature and high-pressure experiments, carried out in neon pressure medium, show that the transition boundary has a positive pressure-temperature slope with $P = -5.0 + 0.070T$ (for pressure in gigapascals and temperature in kelvin).

At higher pressure, we carried out two experiments on FeO without a pressure medium. The two experiments were identical in experimental configuration but different in the pressure and temperature ranges. We observed no phase transition between 16 and 84 GPa at room temperature, consistent with previous static compression experiments (*5*). Upon heating, new diffraction peaks started to appear at 74 GPa and 900 K in the first experiment and at 90 GPa and 600 K in the second experiment. In the first experiment, the diffraction peaks from the new phase became more intense with

Geophysical Laboratory and Center for High-Pressure Research, 5251 Broad Branch Road, N.W., Washington, DC 20015, USA.

increasing temperature and pressure, but the diffraction peaks from the rhombohedral phase were observable even at 1100 K and 80 GPa. The sample was not recovered from the experiment because the diamond anvil broke in the attempt to obtain higher pressure. In the second experiment, the transition was completed at 96 GPa and 800 K. To observe the transition in reverse, we isothermally decompressed the sample at 900 K. The back transition from the high-pressure phase to the rhombohedral phase was not observed during the decompression. Instead, the high-pressure phase transformed directly back to the cubic phase at 45 GPa. The lattice parameter of the recovered sample was $a_0 = 4.324 \pm 0.001$ Å, virtually the same as that of the starting material (9), $a_0 = 4.323 \pm 0.001$ Å. On the basis of the two high-pressure and high-temperature experiments, the transition from the rhombohedral phase to the high-pressure phase has a negative pressure-temperature slope with $P = 118.0 - 0.051T$. A triple point is therefore inferred to occur at 66 ± 3 GPa and 1020 ± 50 K (Fig. 1).

The diffraction pattern of the high-pressure phase consists of six observable diffraction peaks between 1.0 and 3.0 Å, which we indexed by using a hexagonal cell (Table 1). The calculations were based on a NiAs-type structure with lattice parameters $a = 2.574(2)$ Å and $c = 5.172(4)$ Å. It is clear that the observed new diffraction lines fit the NiAs structure (B8) well. The density variation of the NiAs phase of FeO is comparable to the variation in shock compression data (Fig. 2). A least squares fit of the static compression data at 900 K to the Birch-Murnaghan equation of state (*10*) yielded isothermal bulk modulus $K_T = 172 \pm 14$ GPa and its pressure derivative $(\partial K_T/\partial P)_T = 4.3 \pm 0.6$ for the high-pressure NiAs phase of FeO.

Our phase diagram of FeO (Fig. 1) suggests that the observed density discontinuity at about 70 GPa along the Hugoniot curve from the shock compression experiment is consistent with the transition from the rock salt (B1) to the NiAs (B8) structure. The NiAs structure of FeO consists of hexagonally close-packed layers of O and Fe alternately stacked along the *c* axis. The structure is closely related to the rock salt structure and can be derived by variation of the stacking along the body diagonal direction (the [111] direction, corresponding to the *c* axis in the NiAs structure) in the rock salt structure (*2, 4, 11*). The NiAs structure can accommodate a greater degree of covalent and metallic bonding by changing its *c*/*a* ratio to bring metal atoms closer together and to create more distorted octahedrons (*3*). The *c*/*a* ratio is a good indicator of the volume change between the rock salt and NiAs structures, and the metal-metal distance reflects the effective radii of the ions. The experimentally determined *c*/*a* ratio for the NiAs phase of FeO is about 2.02 ± 0.01, substantially larger than the ideal value of 1.63. However, the result, in general, is consistent with the correlation between *c*/*a* ratio and the difference in cation-anion electronegativity (*2*).

A density discontinuity exists along the Hugoniot of FeO in the shock compression experiments (*1, 6*). However, the density change between the high- and low-pressure phases of FeO, derived from the shock compression data, has been uncertain because of the ambiguity in defining the phase boundary. Jeanloz and Ahrens (*1*) calculated a density increase of 4% at 70 GPa for the shock-induced transition, whereas Jackson and co-workers (*2, 4*) argued that the density increase could be as high as 14 to 20% if the 101-GPa datum (compare with Fig. 2) was not used in characterization of the high-pressure phase. The uncertainty in the density increase across the shock-induced transition resulted in a wide range of hypotheses on the nature of the transition (*1–4, 12*). It has been proposed that the densification is caused by a phase transition either from rock salt (B1) to CsCl (B2) or from rock salt to NiAs structures, a spin-pairing transition, or a Mott transition. Our experimental results show that the high-pressure phase has a NiAs structure. The density of the NiAs phase of FeO, determined from x-ray diffraction data, indicates that the 101-GPa datum in the shock wave experiment (*1*) is consistent with the density of the high-pressure NiAs phase (Fig. 2). The density increase across the transition, determined from our static compression data, is about 4%, consistent with the original evaluation of the shock compression data (*1*). The 4% density increase can be explained by geometric rearrangement from rock salt to NiAs structures and the measured *c*/*a* ratio of the NiAs phase (*4*). Based on the measured *c*/*a* ratio of the NiAs phase of FeO, the Fe–Fe distance in the NiAs structure is about 8% shorter than that in the rock salt structure. The Fe–Fe

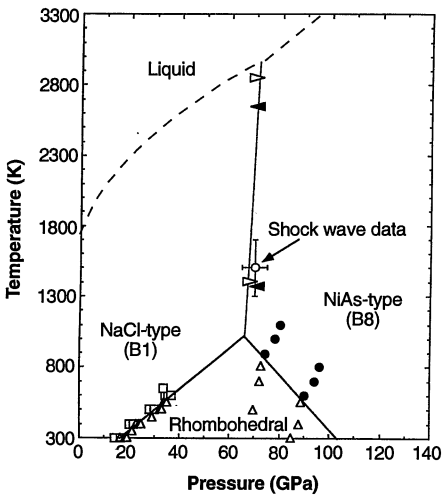

Fig. 1. Experimentally determined phase diagram of FeO. Data are shown by symbols: open squares, rock salt structure (B1); open triangles, rhombohedral phase; and solid circles, NiAs-type structure (B8). The shock-induced transition point (*1*) is represented by an open circle. The open and solid arrows indicate metallization of FeO inferred from electrical resistance measurements in the laser-heated diamond-anvil cell (*21*). The melting curve (dashed curve) is from laser-heating experiments in the diamond-anvil cell (*22*). A higher melting temperature at high pressure has also been reported (*21*).

Table 1. Observed and calculated x-ray diffraction pattern of FeO at 96 GPa and 800 K.

h	*k*	*l*	d_{obs}	d_{cal}*	$d_{obs} - d_{cal}$	I_{obs}†
0	0	2	2.594	2.586	0.008	s
1	0	0	2.224	2.229	−0.005	m
1	0	1	2.043	2.047	−0.004	s
1	0	2	1.686	1.688	−0.002	vs
0	0	4	1.293	1.293	0.000	mw
1	1	2	1.153	1.152	0.001	mw

*Hexagonal unit cell: $a = 2.574(2)$ Å and $c = 5.172(4)$ Å, which gives $c/a = 2.01$. †The relative intensities of the peaks are described as strong (s), medium (m), very strong (vs), and medium weak (mw).

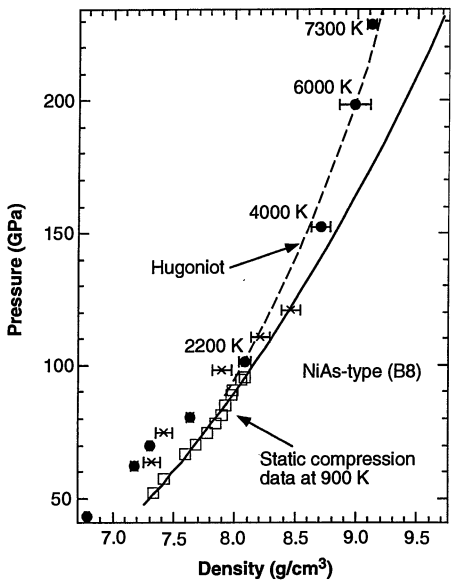

Fig. 2. Densities of the high-pressure NiAs phase of FeO as a function of pressure at 900 K compared with the shock compression data. Our static compression data are shown by the open squares; the size of the symbols represents the uncertainties in pressure and density. Hugoniot data are shown by the solid circles (*1*) and crosses (*6*). Hugoniot temperatures (*1*) are indicated by numbers. The dashed and solid curves are the calculated shock compression curve (*1*) and the best fit to the static compression data at 900 K, respectively.

bonding in FeO becomes more important at high pressure. The shorter Fe–Fe distance across shared FeO_6 octahedral faces in the NiAs structure could lead to metallic conductivity in FeO by electron delocalization. The metallization will also be enhanced by the loss of local Fe moments (*13*).

Earth's core is about 10% less dense than pure iron at core pressures and temperatures (*14*). This density deficit implies that a substantial amount of light elements, such as H, O, S, C, Si, or Mg, is incorporated into the core. Although there is no simple answer to what light elements may be present in the core, recent experimental results on the solubility of FeO in molten iron (*15–18*) and the metallization of FeO (*19–20*) at high pressure and temperature imply that oxygen is the alloying element. The covalently and metallically bonded NiAs-type structure of FeO at high pressure would allow some solubility of oxygen (in the form of FeO) in molten iron.

FeO is the only monoxide that has been found to have covalently and metallically bonded NiAs structure at high pressure and temperature, contrary to CaO, SrO, and BaO, which transform from rock salt (B1) to CsCl (B2) structures. The changes in the structure and the nature of chemical bonding in FeO would allow FeO to form solid solutions with compounds of similar structure and bonding, such as FeS and Fe (hexagonal closest packing), at high pressure and temperature. This opens the possibility of incorporating both oxygen and sulfur in the Earth's core.

REFERENCES AND NOTES

1. R. Jeanloz and T. J. Ahrens, *Geophys. J. R. Astron. Soc.* **62**, 505 (1980).
2. I. Jackson and A. E. Ringwood, *ibid.* **64**, 767 (1981).
3. A. Navrotsky and P. K. Davies, *J. Geophys. Res.* **86**, 3689 (1981).
4. I. Jackson, S. K. Khanna, A. Revcolevschi, J. Berthon, *ibid.* **95**, 21671 (1990).
5. T. Yagi, T. Suzuki, S. Akimoto, *ibid.* **90**, 8784 (1985).
6. T. Yagi, K. Fukuoka, H. Takei, Y. Syono, *Geophys. Res. Lett.* **15**, 816 (1988).
7. H. K. Mao *et al.*, *J. Geophys. Res.* **96**, 8069 (1991).
8. Y. Fei, H. K. Mao, J. Shu, J. Hu, *Phys. Chem. Miner.* **18**, 416 (1992). High pressures were generated in a Mao-Bell–type diamond-anvil cell made of the alloy Inconel. High temperature was achieved with a small molybdenum wire resistance heater positioned around the diamond anvils and a large heater fitted around the protruding portion of the piston-cylinder. The double-heater configuration has the advantage of achieving higher pressures and temperatures simultaneously and reducing the axial temperature gradient. Temperatures were measured with a platinum-rhodium thermocouple, and pressures were determined by measuring the lattice parameter of gold, on the basis of its equation of state [O. L. Anderson, D. G. Isaak, S. Yamamoto, *J. Appl. Phys.* **65**, 1534 (1989)].
9. The starting material of FeO was synthesized from a mixture of $Fe_{0.947}O$ and metallic Fe at 9 GPa and 1273 K in a multianvil apparatus. The lattice parameter of the synthesized sample was a_0 = 4.323 Å, corresponding to composition $Fe_{0.98}O$ [R. M. Hazen and R. Jeanloz, *Rev. Geophys. Space Phys.* **22**, 37 (1984)].
10. F. Birch, *J. Geophys. Res.* **83**, 1257 (1978).
11. W. B. Pearson, *The Crystal Chemistry and Physics of Metals and Alloys* (Wiley-Interscience, New York, 1972).
12. D. M. Sherman, *Geophys. Res. Lett.* **16**, 515 (1989).
13. D. G. Isaak, R. E. Cohen, M. J. Mehl, D. J. Singh, *Phys. Rev. B* **47**, 7720 (1993).
14. F. Birch, *J. Geophys. Res.* **69**, 4377 (1964).
15. T. Kato and A. E. Ringwood, *Phys. Chem. Miner.* **16**, 524 (1989).
16. E. Ohtani and A. E. Ringwood, *Earth Planet. Sci. Lett.* **71**, 85 (1984); ——— and W. Hibberson, *ibid.*, p. 94.
17. A. E. Ringwood and W. Hibberson, *Phys. Chem. Miner.* **17**, 313 (1990).
18. ———, *Earth Planet. Sci. Lett.* **102**, 235 (1991).
19. E. Knittle and R. Jeanloz, *Geophys. Res. Lett.* **13**, 1541 (1986).
20. ———, A. C. Mitchell, W. J. Nellis, *Solid State Commun.* **59**, 513 (1986).
21. E. Knittle and R. Jeanloz, *J. Geophys. Res.* **96**, 16169 (1991).
22. R. Boehler, *Earth Planet. Sci. Lett.* **111**, 217 (1992).

23. We thank C. M. Bertka, R. E. Cohen, L. W. Finger, R. J. Hemley, R. Jeanloz, A. Navrotsky, and C. T. Prewitt for discussions and comments. Supported by the NSF Center for High-Pressure Research and the Carnegie Institution of Washington.

7 September 1994; accepted 1 November 1994

The Accumulation Record from the GISP2 Core as an Indicator of Climate Change Throughout the Holocene

D. A. Meese,* A. J. Gow, P. Grootes, P. A. Mayewski, M. Ram, M. Stuiver, K. C. Taylor, E. D. Waddington, G. A. Zielinski

A depth-age scale and an accumulation history for the Holocene have been established on the Greenland Ice Sheet Project 2 (GISP2) deep core, providing the most continuously dated record of annual layer accumulation currently available. The depth-age scale was obtained with the use of various independent techniques to count annual layers in the core. An annual record of surface accumulation during the Holocene was obtained by correcting the observed layer thicknesses for flow-thinning. Fluctuations in accumulation provide a continuous and detailed record of climate variability over central Greenland during the Holocene. Climate events, including "Little Ice Age" type events, are examined.

The GISP2 ice core was drilled from surface to bedrock to obtain a paleoclimatic history spanning the last 200,000 years. The summit drilling site is located at 72.6°N, 38.5°W, at an elevation of 3200 m. A European companion study, the Greenland Ice Core Project, has obtained a parallel ice core at a site approximately 30 km east of the GISP2 site. The Holocene accumulation record (*1*) from the GISP2 core provides a continuous, detailed history of climate fluctuations over central Greenland. In this report we describe the accumulation record spanning the last 11,000 years (Holocene) and its relation to climate change (*2*) but we make no comparison with other records, which tend to vary.

Although the degree of climate change during the Holocene has been small in comparison to events such as the Younger Dryas, the events that have taken place are important to our understanding of future changes and the effect they may have on our society. Although the accumulation record cannot necessarily answer these questions, it can provide initial detailed information on when climate changes have occurred. In addition, layer thickness (accumulation) as determined in the field also provides investigators with immediate information on where to sample the core in detail.

We dated the ice core throughout the top 1640 m by identifying and counting annual layers using a number of physical and chemical parameters, including measurements of visual stratigraphy (*3*), electrical conductivity (ECM) (*4*), laser light scattering (from dust) (*5, 6*), oxygen isotopes, and chemistry. Each of these parameters exhibits a distinct seasonal signal. The definitive summer stratigraphic signal at the GISP2 site throughout the Holocene is coarse-grained depth hoar (*3*). These layers are easily recognized in a core examined in transmitted light. Annual stratigraphic layers are visible to a minimum of 55,000 cal B.P. (equivalent to calendar years before the present).

A relation between $\delta^{18}O$ and surface

D. A. Meese and A. J. Gow, Cold Regions Research and Engineering Laboratory, 72 Lyme Road, Hanover, NH 03755, USA.
P. Grootes and M. Stuiver, Quaternary Isotope Laboratory, University of Washington, Seattle, WA 98195, USA.
P. A. Mayewski and G. A. Zielinski, Glacier Research Group, Institute for the Study of Earth, Oceans, and Space, University of New Hampshire, Durham, NH 03824, USA.
M. Ram, Department of Physics, State University of New York at Buffalo, Amherst, NY 14260, USA.
K. C. Taylor, Desert Research Institute, Reno, NV 89506, USA.
E. D. Waddington, Department of Geophysics, University of Washington, Seattle, WA, 98195, USA.

*To whom correspondence should be addressed.